Applied Catalysis B: Environmental 160–161 (2014) 684–691

Contents lists available at ScienceDirect

Applied Catalysis B: Environmental

journal homepage: www.elsevier.com/locate/apcatb

Supercritical water syntheses of Ce_xTiO_2 nano-catalysts with a strong metal-support interaction for selective catalytic reduction of NO with NH_3

Yue Liu[a], Weiyuan Yao[a], Xiaoli Cao[a], Xiaole Weng[a,*], Yan Wang[a], Haiqiang Wang[a], Zhongbiao Wu[a,b,*]

[a] Department of Environmental Engineering, Zhejiang University, 388 Yuhangtang Road, Hangzhou 310058, PR China
[b] Zhejiang Provincial Engineering Research Center of Industrial Boiler & Furnace Flue Gas Pollution Control, 388 Yuhangtang Road, Hangzhou 310058 PR China

ARTICLE INFO

Article history:
Received 17 March 2014
Received in revised form 15 May 2014
Accepted 16 June 2014
Available online 21 June 2014

Keywords:
Supercritical water
SCR
Nitrogen oxide
Strong metal-support interaction
DRIFT

ABSTRACT

This paper reported the feasibility of a supercritical water synthesis route (referred as CHFS) in the application of selective catalytic reduction (SCR) of NO with NH_3. A series of well-reported Ce_xTiO_2 SCR catalysts were synthesized and then subjected to a range of characterizations (e.g. XRD, XPS, H_2-TPR, HADDF, etc.). Experimental results revealed that the unusual and rapid crystallizing environment of the CHFS route had resulted in a highly dispersed CeO_2 and a strong metal-support interaction (SMSI) for Ce_xTiO_2 catalysts, which promoted the enriched surface oxygen vacancies and facilitated the formation of NO_2 and nitrite species over the catalyst surface, effectively enhancing their SCR performances. Amongst the developed Ce_xTiO_2 catalysts, $Ce_{0.25}TiO_2$ revealed the highest SCR activity with more than 90% NO conversion being achieved in a broad temperature range of 240–440 °C. Such broad temperature window was proven due to the SMSI, which lowered the NH_3 oxidation ability of CeO_2, retaining the effective utilization of NH_3 throughout the SCR process. The work conducted herein demonstrates the feasibility of the CHFS route in the syntheses of SMSI catalysts for SCR application and also explores the SCR reaction mechanism over the well-reported Ce_xTiO_2 catalysts. We expected that this work could shed some lights on the development of feasible preparative routes for the syntheses of advanced SMSI catalysts for SCR application.

1. Introduction

Currently, the control of NO_x emissions from coal-fired flue gasses has become an important task for many developing countries due to the increasing impact of the NO_x on urban smog, acid rain, ozone depletion, greenhouse effect, etc. Selective catalytic reduction (SCR) of NO_x into harmless N_2 and H_2O has generally recognized as one of the most desirable and attractive ways for NO_x removal. Although catalysts like WO_3–V_2O_5/TiO_2 [1] and MoO_3–V_2O_5/TiO_2 [2] have been well commercialized for industrial SCR application, these vanadium-based catalysts are generally suffered from environmental poisoning issue (i.e. the vanadium is very harmful to ecological environment), which leads to a strong incentive for the researchers to search for highly active and relatively "green" catalysts for SCR application.

In literature, there were numerous works having been conducted to develop such alternative SCR catalysts [3–6]. However, these works more focused on adjusting the compositions and screening more active components (these are generally expensive) for the catalysts to yield superior SCR performance, while studies on feasible preparative methods seemed being given very little care. As a matter of fact, the physical/chemical properties of the catalysts are strongly relied on the preparative routes, where for composition–identical catalysts, their particle morphologies,

Abbreviations: CHFS, continuous hydrothermal flow synthesis; SC–Ce_xTiO_2, Ce_xTiO_2 catalysts that were synthesized via the CHFS method; WI–Ce_xTiO_2, Ce_xTiO_2 catalysts that were synthesized via a wet impregnation method; DM–Ce_xTiO_2, Ce_xTiO_2 catalysts that were synthesized via a dry mixing method; CP–Ce_xTiO_2, Ce_xTiO_2 catalysts that were synthesized via a co-precipitation method; SMSI, strong metal-support interaction.

* Corresponding authors at: Zhejiang University, Department of Environmental Engineering, 388 Yuhangtang Road, Hangzhou 310058, PR China.
Tel.: +86 571 88982034; fax: +86 571 88982034.
E-mail addresses: xlweng@zju.edu.cn (X. Weng), zbwu@zju.edu.cn (Z. Wu).

http://dx.doi.org/10.1016/j.apcatb.2014.06.022
0926-3373/

surface areas and active species dispersion could be significantly varied with different preparative routes. As such, studies on feasible preparative methods, which can offer better activities for conventional SCR catalysts would be very necessary [7].

Following the pioneering researches of Arai Group [8–10], a continuous hydrothermal (using supercritical water) flow synthesis (hereafter referred as CHFS) method has been constantly explored for the syntheses of advanced nano-catalysts. This process used a flow of supercritical (sc) water (critical temperature $T_c = 374\,^{\circ}C$; critical pressure $P_c = 22.1$ MPa) that reacted with a flow of chosen metal salts (in an aqueous solution) to give rapid precipitation and controlled growth of nano-particles [11]. The method had resulted in a wide ranging outcome for its products in terms of high surface area [12–15], defective crystallines [16], homogenous dispersion of active species [17], etc. However, to the best of our knowledge, there is no report of this method utilized for the production of advanced catalysts for SCR application.

Recently, we report an initial finding that the CHFS route could result in a strong metal-support interaction (SMSI) for $Pd/Ce_xZr_{1-x}O_2$ catalyst, which had promoted a low-temperature activation of molecular oxygen and yielded a total oxidation temperature for toluene removal at as low as 145 °C [18]. Since there are few reports on the effects of SMSI in SCR process [19,20], in this paper, we visited a well-reported SCR catalyst, $Ce_xTi_{1-x}O_2$ [7,19,21–25], studying the feasibility of the CHFS route for the syntheses of conventional SCR catalysts with better performances. The paper will focus on analyzing the possible occurrence of SMSI in the resulted $Ce_xTi_{1-x}O_2$ catalysts and investigating how the SMSI affects the performance of these catalysts during the SCR reaction.

2. Experimental

2.1. Materials

$[(NH_4)_2Ce(NO_3)_6$, ≥99.9%] and nano-sized anatase TiO_2 (5–10 nm, 99.8% metal basis) were purchased from Aladdin Reagent Co., Ltd (Shanghai, PR China). Titanium (IV) bis (ammonium lactate) dihydroxide $[CH_3CH(O—)CO_2NH_4]_2Ti(OH)_2$ (50 wt% in water) was supplied from Alfa Aesar company (UK). All chemicals were used as obtained. Deionized water was used in all experiments.

2.2. Catalysts characterizations

Freeze–drying was performed using a Vacuum Freeze Dryer, Model LGJ-10C, supplied from Beijing Boyikang Laboratory Instruments Co., Ltd; the solids were frozen for 4 h and then freeze-dried for 24 h at 10 Pa. The dispersion of the catalysts were investigated using a model Tecnai G^2 F20 S-TWIN (FEI Company, USA) high-resolution transmission electron microscope (HR-TEM, 400 kV accelerating voltage) instrument equipped with STEM and HAADF. Energy dispersive X-ray (EDX) elemental analysis was conducted using a SIRION-100 scanning electron microscope with a GENESIS4000 X-ray energy dispersive spectroscopy. X-ray powder diffraction was conducted using a Rigaku D/Max RA diffractometer with Cu $K\alpha$ radiation ($\lambda = 0.15418$ nm) at 40 kV and 150 mA and at an angle of 2θ from 10° to 80°. Laser Raman spectra were obtained using a LABRAM-HR Ramas-cope fitted with a spectraphysics argon ion laser ($\lambda = 514$ nm) at a power of 20 mW. BET-BJH was determined using N_2 physisorption at 77 K, with a Micromeritics ASSP 2020 equipment. Catalyst degassing pre-treatment was conducted at 300 °C for 1 h under a vacuum in order to remove any adsorbed species. X-ray photoelectron spectroscopy (XPS) was conducted to analyze the surface atomic state of the catalysts with Al $K\alpha$ X-rays (Thermal, ESCALAB 250). The shift of the binding energy due to relative surface charging was corrected using C 1s level at 284.6 eV as an internal standard.

Temperature programmed reduction (TPR) was performed on a custom-made thermal conductivity detector (TCD) setup (TP-5079, TianJin Xianquan Co. Ltd., PR China) using 100 mg catalysts. After pretreated in He gas flow at 400 °C for 1 h, the catalysts were cooled to room temperature at a flow rate of 30 mL/min for about 30 min. The reduction process was carried out under a flow of pure H_2 at a heating rate of 10 °C/min from 100 °C to 800 °C.

FT-IR was conducted using an in situ DRIFT cell with an appliance of a gas flow system. The DRIFT measurements were performed with ZnSe windows coupled to Bruker tensor 27 FTIR spectrometers. In the DRIFT cell, catalysts were pretreated at 400 °C in a He environment for 2 h, and then cooled to 250 °C. The background spectrum was recorded with flowing He and was subtracted from the catalyst spectrum.

2.3. Selective catalytic reduction (SCR) activity measurements

Selective catalytic reduction (SCR) of NO with NH_3 was carried out in a fixed-bed reactor. The experiments were performed under atmospheric pressure at 200–440 °C. The reactor consisted of a quartz tube of 1 cm i.d. in which 0.5 g of catalyst was filled and a water bubbler to provide ca. 5 vol% H_2O for reaction system. A type K thermocouple was placed at the centre of the bed for temperature measurement. The typical reactant gas composition was as follows: 600 ppm NO, 600 ppm NH_3, 3.5% O_2, 5 vol% H_2O and balance N_2. The gas hourly space velocity (GHSV) was kept at about 150,000 h^{-1} for this system. NO, NO_2, N_2O and O_2 concentration were monitored by an infrared gas analyzer (Photon II, Madur Electronics, Austria).

2.4. General syntheses

2.4.1. CHFS method

The Ce_xTiO_2 catalysts were manufactured in our laboratory using a continuous hydrothermal flow system (CHFS). The details of these syntheses have been reported in our previous publication [26]. The resulted catalyst is hereafter referred as SC–Ce_xTiO_2.

2.4.2. Wet-impregnation method

The Ce_xTiO_2 nano-catalyst was prepared by introducing the cerium nitrate solution into nano-sized anatase TiO_2 support via a conventional wet impregnation route. The mixture was stirred for 6 h, dried at 80 °C for 18 h and then calcined at 450 °C for 1 h to get the desired catalysts for further analysis. The resulted catalyst is hereafter referred as WI–Ce_xTiO_2.

2.4.3. Dry-mixing method

The Ce_xTiO_2 nano-catalyst was prepared by dry mixing the CHFS-made CeO_2 and TiO_2 nano-particles in a planetary ball mill (XQM2 by NJU-KX) with stainless steel container and balls. Seven big balls (10 mm) and 34 small balls (5.8 mm) were used together in grinding process. The mixing was run at 250 rpm for 24 h. The resulted catalyst is hereafter referred as DM–Ce_xTiO_2.

2.4.4. Co-precipitation method

The Ce_xTiO_2 nano-catalyst was prepared by introducing $NH_3{\cdot}H_2O$ solution (25%) into a stoichiometric solution (100 mL) of $Ce(NO_3)\,6H_2O$ and $Ti(SO_4)_2$ under vigorous agitation until pH = 10 [19]. The suspension was aged in air for 3 h at room temperature

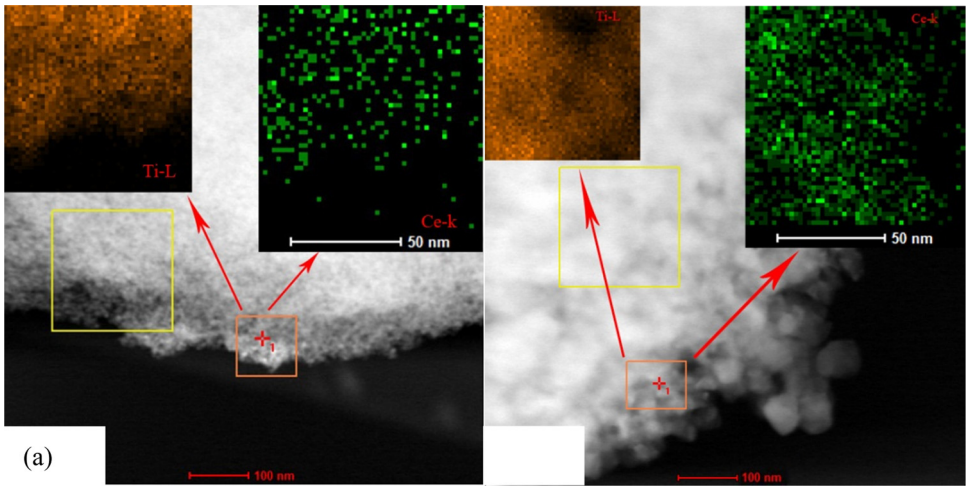

Fig. 1. EDX mapping images of (a) SC–$Ce_{0.05}TiO_2$ and (b) WI–$Ce_{0.05}TiO_2$ catalysts.

and atmospheric pressure. The resultant precipitates were dried at 110 °C overnight and calcined at 500 °C for 5 h in air. The yielded catalyst is hereafter referred as CP–Ce_xTiO_2.

3. Results and discussion

3.1. Constitutions and BET surface areas of the SC–Ce_xTiO_2 catalysts

The constitutional molar ratios of SC–Ce_xTiO_2 (where $x = 0.05$, 0.10, 0.25, 0.5, 0.75, 1.0) catalysts were evaluated using a calibrated EDX (10 area scans) and gave the average Ce:Ti molar ratios at 0.05, 0.10, 0.20, 0.42, 0.70, 0.94, respectively, which were relatively close to their expected stoichiometries. The slight variations in Ce:Ti molar ratio could be attributed to the varied yields of cerium and titanium ions during their precipitations from the supercritical water.

BET-BJH measurements were conducted to exclude the surface areas of the resulted SC–Ce_xTiO_2 catalysts. As shown in Table 1, the surface areas of SC–Ce_xTiO_2 catalysts were initially not changed with the Ce contents, but were significantly decreased after the Ce content approach 0.75. This is unsurprising given that the more presence of CeO_2 over the TiO_2 support, the ease of these CeO_2 phase aggregation or separation occurred. Amongst these catalysts, the SC–$Ce_{0.25}TiO_2$ catalyst revealed the highest pore size and pore volume. One may argue that the BET surface areas present herein were not consistent with our previous publication [26]. This is mainly due to their varied pre-treatment conditions (i.e. 80 °C versus 300 °C) as the latter could ensure the complete removal of any adsorbed species to yield more reliable BET values for the catalysts.

Table 1
BET-BJH results of the SC–Ce_xTiO_2 catalysts.

Catalysts	Surface area (m^2/g)	Pore volume (cm^3/g)	Pore size (Å)
$Ce_{0.05}TiO_2$	198.9	0.39	58.53
$Ce_{0.1}TiO_2$	189.5	0.39	60.40
$Ce_{0.25}TiO_2$	185.7	1.23	217.28
$Ce_{0.5}TiO_2$	220.8	0.33	58.93
$Ce_{0.75}TiO_2$	113.4	0.38	111.63
$Ce_{1.0}TiO_2$	87.0	0.38	151.28

3.2. Dispersion of CeO_2 over the TiO_2 support

To demonstrate that the varied preparative routes could result in different physical/chemical properties for their products, the active specie dispersion was evaluated where the catalyst with the lowest Ce content (i.e. SC–$Ce_{0.05}TiO_2$) were selected for comparing to a composition-identical WI–$Ce_{0.05}TiO_2$ catalyst. High-angle annular dark-field scanning transmission electron microscopy (HAADF STEM) with the benefit of its great sensitivity to atomic number (and better contrast than the dark and bright field operation modes[27]) was employed to evaluate the dispersion of CeO_2 over the TiO_2 support. Fig. 1a and b shows the EDX mapping images (at ca. 100 × 100 nm scanning region) of the $Ce_{0.05}TiO_2$ catalysts. For SC–$Ce_{0.05}TiO_2$ catalyst, the CeO_2 (green dots/rods) was observed highly dispersed over the TiO_2 support. This is unsurprising given that the simultaneous co-precipitation of Ce and Ti metal ions from the supercritical water (SC–H_2O) could yield a highly dispersed CeO_2 over the TiO_2 support [17]. In contrast, the WI–$Ce_{0.05}TiO_2$ catalyst revealed a relatively aggregated green dots/rods, showing a comparatively poor dispersion of CeO_2. This result revealed the advantage of the CHFS route in the synthase of highly dispersed nano-catalysts, which might give rise to superior performance in SCR application.

3.3. Selective catalytic reduction (SCR) activity measurements

Fig. 2 illustrated the NO conversion within the temperature range of 200–440 °C for SC–Ce_xTiO_2 catalysts. As expected, the addition of Ce had effectively promoted the SCR performance as all the SC–Ce_xTiO_2 catalysts had showed superior performances than the SC–TiO_2 catalyst. Among these catalysts, the SC–$Ce_{0.25}TiO_2$ catalyst revealed the highest SCR activity, where more than 90% NO conversion was achieved in the temperature range of 240–440 °C, showing a rather broad temperature window for NH_3-SCR process. No obvious N_2O production was detected within the investigated temperature range for all SC–Ce_xTiO_2 catalysts, revealing an excellent N_2 selectivity for the catalysts.

In literature, He et al. [7] had reported a modified precipitation route for the syntheses of Ce_xTiO_2 catalysts, which revealed excellent low-temperature SCR activity comparing to those reported by Xu et al. [23] and Gao et al. [25]. The catalysts had yielded more than 90% NO conversion (under a similar GHSV of 150,000 h^{-1}) in the temperature range of 250–350 °C. Here, our SC–$Ce_{0.25}TiO_2$ catalyst showed a slightly better SCR activity (90% NO conversion within 240–440 °C) but with a much broader temperature window.

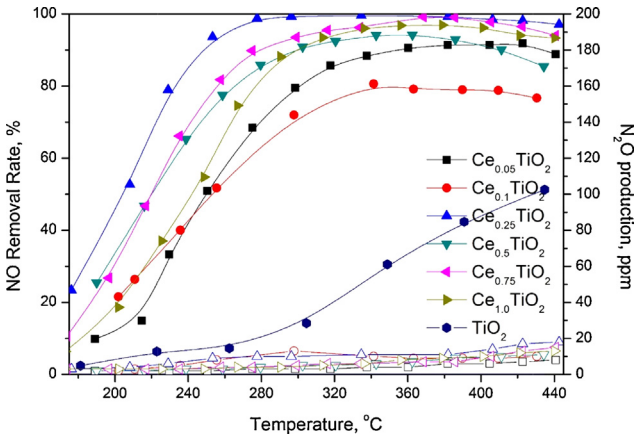

Fig. 2. SCR activities and N_2 selectivity of SC–Ce_xTiO_2 and SC–TiO_2 catalysts. ([NH_3] = [NO] = 600 ppm, [O_2] = 3%, [H_2O] = 5 vol%, N_2 balance, GHSV = 150,000 h^{-1}), where solid symbols for SCR activities and hollow symbols for N_2O production.

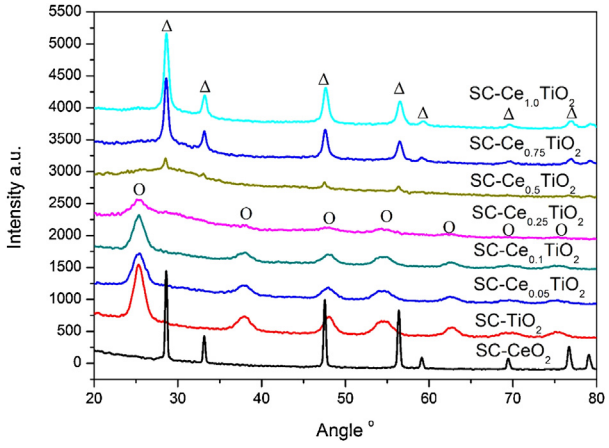

Fig. 3. X-ray diffraction patterns of SC–Ce_xTiO_2, SC–TiO_2 and SC–CeO_2 catalysts, where O = anatase TiO_2 and Δ = CeO_2.

3.4. X-ray powder diffraction

To clarify the possible causes of the SC–Ce_xTiO_2 catalysts for their remarkable SCR performances, X-ray powder diffraction (XRD) was then utilized to get insight into the crystalline information of these catalysts. As shown in Fig. 3, the SC–$Ce_{0.05}TiO_2$ and SC–$Ce_{0.1}TiO_2$ catalysts both revealed the characteristic peaks of anatase TiO_2 (JCPDS 21-1272) where no extra peaks assigned to CeO_2 (PDF-ICDD34-0394) were observed. This might indicate a superior dispersion or an incorporation of CeO_2 into the TiO_2 support for the catalysts. With the accumulation of Ce content, the fluorite CeO_2 peaks became more intense while the anatase TiO_2 peaks tended to be weakened and eventually disappeared in the SC–$Ce_{0.75}TiO_2$ and SC–$Ce_{1.0}TiO_2$ catalysts. Li et al. [19] had reported that the formation of Ce–Ti amorphous oxides could induce a short-order Ce–O–Ti species due to the strong interaction between the CeO_2 and TiO_2 in atomic scale, which would greatly enhance the NH_3-SCR performance. From Fig. 3, it can be clearly seen that the SC–$Ce_{0.25}TiO_2$ was in a "transition region" amongst the SC–Ce_xTiO_2 catalysts, also showing a more than likely amorphous characteristic with the highest pore size and pore volume (see BET results). As such, it is reasonable to believe that this catalyst might possess a strong interaction between the CeO_2 and TiO_2, which hence resulted in a remarkable activity for SCR application (see Fig. 2).

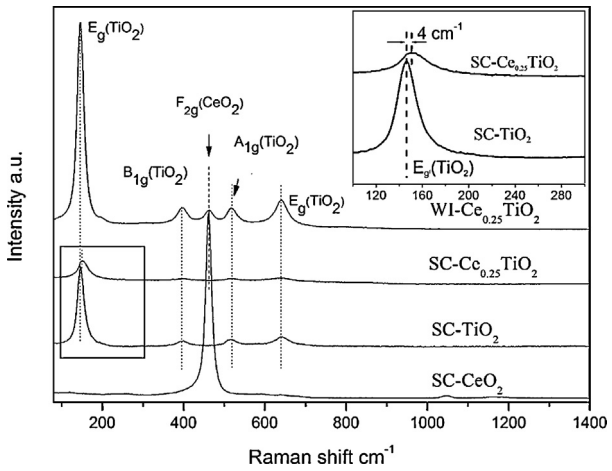

Fig. 4. Raman spectra (n = 514 nm) of WI–$Ce_{0.25}TiO_2$, SC–$Ce_{0.25}TiO_2$, SC–TiO_2 and SC–CeO_2 catalysts.

3.5. Raman measurements

To clarify the existence of any strong interaction between the CeO_2 and TiO_2 in the SC–$Ce_{0.25}TiO_2$ catalyst, this catalyst was then selected for laser Raman characterization. As shown in Fig. 4, the SC–$Ce_{0.25}TiO_2$ showed Four Raman active modes of $2E_g + B_{1g} + A_{1g}$ symmetry, which were assigned to anatase TiO_2 [28]. No F_{2g} mode for CeO_2 at ca. 465 cm^{-1} [29] was observed, implying that the CeO_2 had been incorporated into the TiO_2 lattice, which was consistent with the XRD result. Furthermore, a slight shift (ca. 4 cm^{-1}) of E_g (TiO_2) peak and a significantly weakened Raman peaks were also observed in the SC–$Ce_{0.25}TiO_2$ catalyst. This demonstrated that there was truly a strong metal-support interaction (SMSI) in this catalyst, which gave rise to severely defective structure and hence resulted in abundant oxygen vacancies, significantly weakened the structure symmetry [30,31].

To further investigate the role of the SMSI in SCR process, we also synthesized a WI–$Ce_{0.25}TiO_2$ catalyst that was with relatively weaker metal-support interaction due to its presence of both TiO_2 and CeO_2 phases (as shown in Fig. 4 and Supplementary Fig. S1 for its XRD result). After subjected to SCR activity measurement, this catalyst yielded a rather poor SCR activity, showing only less than 60% NO conversion within the investigated temperature range (see Supplementary Fig. S2). One may argue that the BET surface area could be a reason for such poor performance as the WI–$Ce_{0.25}TiO_2$ catalyst only had a surface area of 40.5 m^2/g, which was four-fold lower than that of SC–$Ce_{0.25}TiO_2$ catalyst (at 185.7 m^2/g). As such, we subsequently dry-mixed the CHFS-made CeO_2 and TiO_2 nanoparticles, yielding a DM-$Ce_{0.25}TiO_2$ catalyst with the surface area of 125.9 m^2/g. After subjected to SCR activity measurement, this catalyst still showed a poor SCR performance and was with even lower SCR activity than that of WI–$Ce_{0.25}TiO_2$ catalyst (see Supplementary Fig. S2). As such, we could conclude that the SMSI did play a significant role in the SCR process.

Following the co-precipitation procedure as reported by Li et al. [19], we further synthesized a CP–$Ce_{0.25}TiO_2$ catalyst with the surface area at 93.0 m^2/g. XRD and Raman analyses had indeed revealed a short-range order of Ce–O–Ti in the catalyst where the XRD result (see Supplementary Fig. S1) clearly indicated an amorphous phase of the catalyst but the Raman result (see Supplementary Fig. S3) revealed the presence of characteristic bands of anatase TiO_2 with the absence of CeO_2 bands. This result was consistent with that reported by Li et al. [19] After subjected to SCR activity measurement, as expected, the CP–$Ce_{0.25}TiO_2$ catalyst revealed a much better SCR performance than either WI–$Ce_{0.25}TiO_2$

Table 2
XPS analyses results of the $Ce_{0.25}TiO_2$ catalysts.

Catalysts	Ce (%)	Ti (%)	Ce/Ti	Ce^{3+}/Ce^{4+}	O (%)			
					O_α (%)	O_β (%)	O_γ (%)	O_β/O_{Total}
WI–$Ce_{0.25}TiO_2$	9.02	14.45	0.62	0.20	43.40	7.99	4.92	0.14
SC–$Ce_{0.25}TiO_2$	3.92	19.47	0.20	0.81	38.38	11.41	5.09	0.21

or DM–$Ce_{0.25}TiO_2$ catalysts but with relatively poorer activity comparing to SC–$Ce_{0.25}TiO_2$ catalyst (see Supplementary Fig. S2). Again, this result confirmed the importance of the SMSI in the SCR reaction.

3.6. XPS analysis

To clarify the surface elemental compositions of $Ce_{0.25}TiO_2$ catalysts, the SC–$Ce_{0.25}TiO_2$ and WI–$Ce_{0.25}TiO_2$ catalysts were then selected for XPS measurements. As shown in Table 2, the SC–$Ce_{0.25}TiO_2$ catalyst revealed a comparable Ce:Ti molar ratio to its stoichiometry where the WI–$Ce_{0.25}TiO_2$ catalyst showed a much higher Ce:Ti molar ratio (at 0.62), implying a severe aggregation of the CeO_2 phase on the catalyst surface, consistent with the HAADF and Raman results.

Fig. 5a shows the XPS spectra of Ce3d for the two catalysts. Generally, the Ce3d spectra were composed of two multiplets (u and v), corresponding to the spin orbit split $3d_{5/2}$ and $3d_{3/2}$ core holes, respectively. As reported previously [25,32], the u_3, u_2, u, v_3, v_2, v peaks were attributed to Ce^{4+} chemical state while the u_1 and v_1 peaks were assigned to Ce^{3+} chemical state. As shown in Table 2, the Ce 3d in the SC–$Ce_{0.25}TiO_2$ catalyst revealed a majority of Ce^{3+} chemical state with the Ce^{3+}/Ce^{4+} molar ratio at 0.81, much higher than that of WI–$Ce_{0.25}TiO_2$ catalyst (at only 0.20). This is unsurprising given that the incorporation of CeO_2 into the TiO_2 lattice could retain significant amounts of Ce^{3+} chemical state on catalyst surface. Since the presence of Ce^{3+} was generally accompanied with oxygen vacancies over the TiO_2 support [33], the SC–$Ce_{0.25}TiO_2$ catalyst is expected to possess abundant oxygen vacancies, hence replenishing remarkable amounts of gaseous oxygen (i.e. chemisorbed oxygen). Indeed, as shown in Fig. 5b and Table 2, the fitted O1s peaks for lattice oxygen O_α (529.0–530.0 eV), chemisorbed oxygen O_β (531.3–531.9 eV) and hydroxyl groups O_γ (532.7–533.5 eV) [34] had revealed that the O_β:O_{Total} molar ratio in SC–$Ce_{0.25}TiO_2$ catalyst was much higher than that of WI–$Ce_{0.25}TiO_2$ catalyst, implying the presence of significant chemisorbed oxygen on the surface. Since such chemisorbed oxygen O_β was very beneficial to SCR process, it is unsurprising given that the SC–$Ce_{0.25}TiO_2$ catalyst would have much higher SCR activity than that of WI–$Ce_{0.25}TiO_2$ catalyst (see Supplementary Fig. S2).

The binding energies of Ti 2p spectra were presented in Fig. 5c, where the peaks at ca. 458.6 eV and 464.3 eV were assigned to $Ti2p_{3/2}$ and $Ti2p_{1/2}$, respectively. As shown in the figure, the WI–$Ce_{0.25}TiO_2$ catalyst did not show any shift from the pure TiO_2 catalyst whiles the SC–$Ce_{0.25}TiO_2$ catalyst revealed a lower binding energy shift. This result further confirmed the strong metal-support interaction (SMSI) between the CeO_2 and TiO_2 in SC–$Ce_{0.25}TiO_2$ catalyst [35].

3.7. H_2-TPR measurements

To investigate the redox properties of Ce_xTiO_2 catalysts, H_2-TPR were then performed. Fig. 6 shows the H_2-TPR profiles of the two catalysts. In a simple approach, for CeO_2-related catalysts, they generally revealed two hydrogen consumption peaks, which could be attributed to the successive reduction of oxygen linked to surface

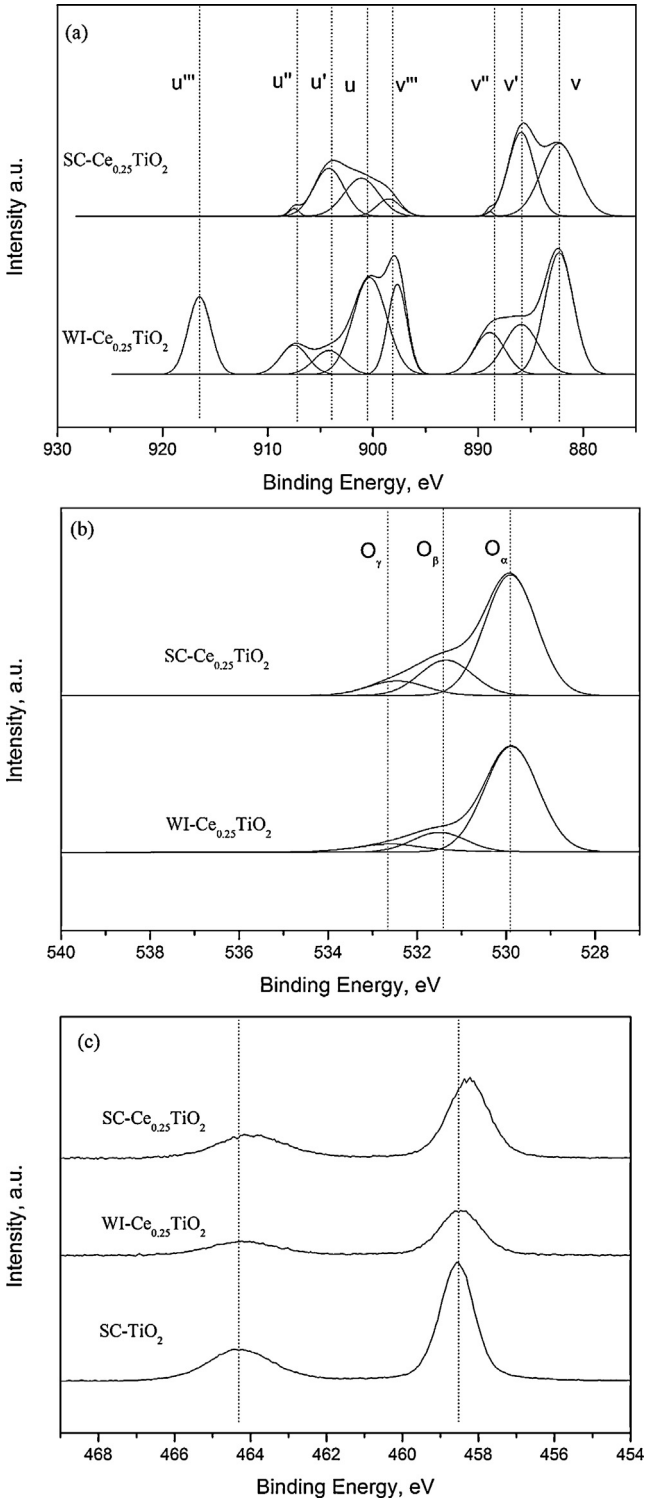

Fig. 5. (a) Ce 3d, (b) O 1s and (c) Ti 2p XPS spectra of WI–$Ce_{0.25}TiO_2$ and SC–Ce_xTiO_2 catalysts.

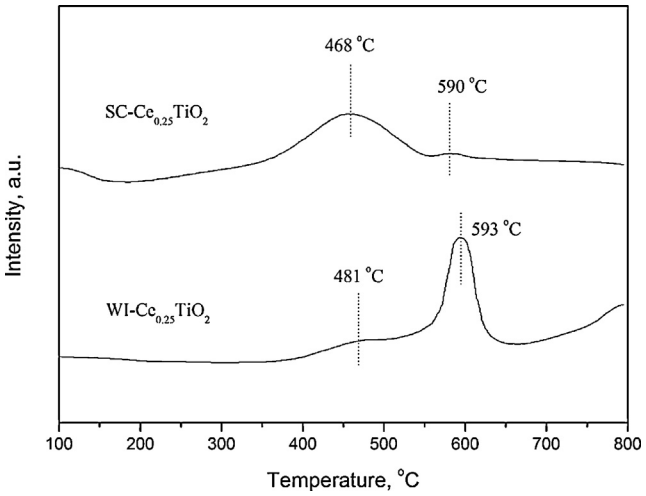

Fig. 6. H_2-TPR profiles profiles of WI–$Ce_{0.25}TiO_2$ and SC–$Ce_{0.25}TiO_2$ catalysts.

and bulk ceria, respectively [36]. For WI–$Ce_{0.25}TiO_2$ catalyst, its surface and lattice oxygen reduction peaks were observed at ca. 481 and 593 °C, respectively, where the latter is more intense than the former, indicating the domination of lattice oxygen reduction for the catalyst. In contrast, the SC–$Ce_{0.25}TiO_2$ catalyst revealed a lower-temperature surface oxygen reduction peak at ca. 468 °C and a similar lattice oxygen reduction peak at ca. 590 °C. However, its former peak showed much boarder and more intense than the latter one, implying that its CeO_2 incorporation could mainly occur at near surface region, retaining enriched surface active oxygen and Ce^{3+} chemical states in the catalyst, consistent with the Raman and XPS results.

3.8. NH_3 oxidation measurements

Since the operation temperature window of the SCR catalysts is strongly related to their NH_3 oxidation abilities [37]. To interpret the board operation temperature window as observed in SC–$Ce_{0.25}TiO_2$ catalyst (see Fig. 2), NH_3 oxidation measurements were then conducted. Fig. 7 illustrated the NH_3 oxidation measurement over the WI–$Ce_{0.25}TiO_2$ and SC–$Ce_{0.25}TiO_2$ catalysts. It can be seen that the WI–$Ce_{0.25}TiO_2$ catalyst revealed a relatively severe NH_3 oxidation within the investigated temperature range whilst for comparison, the SC–$Ce_{0.25}TiO_2$ catalyst only showed little NH_3

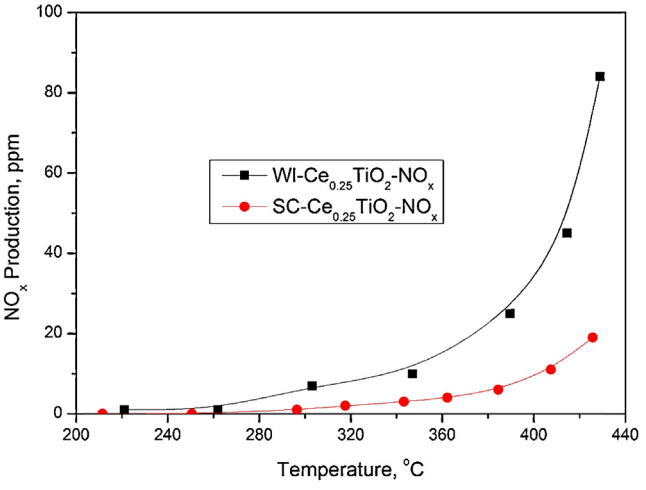

Fig. 7. NH_3 oxidation measurements for WI–$Ce_{0.25}TiO_2$ and SC–$Ce_{0.25}TiO_2$ catalysts ([NH_3] = 800 ppm, [O_2] = 3%, N_2 balance, GHSV = 150,000 h^{-1}).

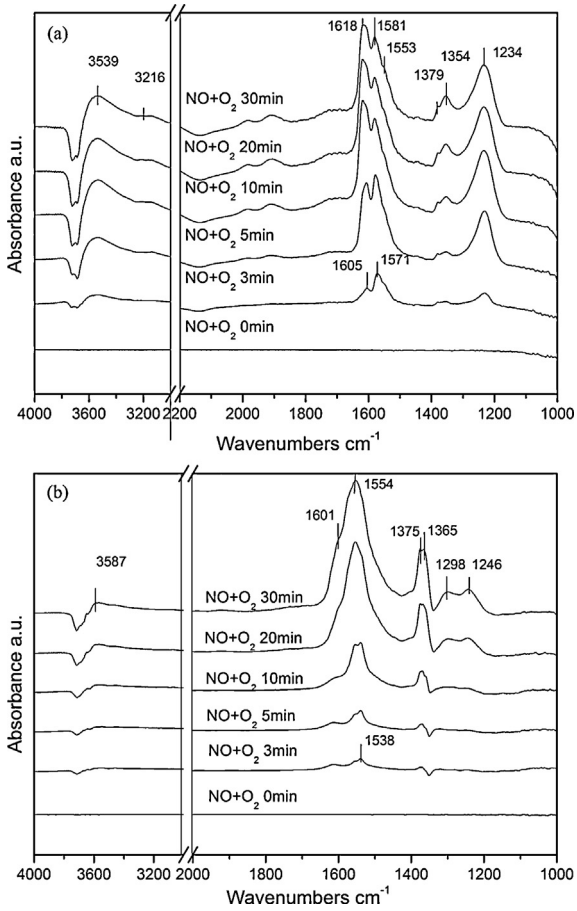

Fig. 8. DRIFT spectra taken at 250 °C upon passing 1000 ppm NO + 3% O_2/He on (a) SC–$Ce_{0.25}TiO_2$ and (b) WI–$Ce_{0.25}TiO_2$ at different time.

oxidation. This result implied that the SMSI could lower the NH_3 oxidation ability of CeO_2 (where pure SC–CeO_2 had shown severe NH_3 oxidation, see Supplementary Fig. S4), which effectively retain the NH_3 utilization throughout the SCR reaction and hence extend the operation temperature window for the SC–$Ce_{0.25}TiO_2$ catalyst.

According to the aforementioned results, it can be concluded that the CHFS route had resulted in a highly dispersed CeO_2 and a SMSI for SC–Ce_xTiO_2 catalysts where the presence of SMSI had led to enriched surface oxygen vacancies on catalyst surface and lowered the NH_3 oxidation throughout the SCR reaction, effectively extending the operation temperature window for the catalysts. Thereafter, further work was then conducted to investigate how the enriched surface oxygen vacancies could promote the SCR reaction.

3.9. DRIFT study

To investigate the SCR mechanism, in situ FITR were then studied. In literature, there are numerous works having reported that some NO_x ad-species and NO_2 can be involved in the SCR reaction via a L–H mechanism, thereby enhancing the SCR performance [38,39]. Furthermore, as a moderate basic material, ceria has been reported being able to provide great numbers of NO adsorption sites, generating significant NO_x ad-species, hence promoting the SCR reaction [40]. To verify the aforementioned observations over our catalysts, NO adsorption over the Ce_xTiO_2 catalysts and the reactivities of these adsorbed species were then investigated.

Fig. 8 showed the DRIFT spectra taken in flowing NO + O_2/He at 250 °C as a function of time on SC–$Ce_{0.25}TiO_2$ (a) and WI–$Ce_{0.25}TiO_2$ (b) catalysts. As indicated in Fig. 8a, a band at 1571 cm^{-1} and weak bands at 1605, 1379, 1354, and 1234 cm^{-1} were detected

for SC–$Ce_{0.25}TiO_2$ catalyst after introduction of NO into the IR cell. With further NO exposure, the band at 1571 cm^{-1} was soon overlapped by bands at 1581 and 1553 cm^{-1}, and a new peak at 1618 cm^{-1} was emerged. In OH stretching region, a negative band at around 3700 cm^{-1} and a positive band at about 3539 cm^{-1} were observed, showing the evidence of H-bonded hydroxyl groups [41,42]. The band located in 1630–1200 cm^{-1} regions were typical nitrate species, and could be attributed to bridged (1605 cm^{-1}) [43], bidentate (1581, 1571 and 1550 cm^{-1}) nitrates [44], respectively. The bands at 1379 and 1354 cm^{-1} could be assigned to *cis*-$N_2O_2^-$ [45,46] and the band at 1234 cm^{-1} may be attributed to nitrite species [46]. The band at 1618 cm^{-1} which rapidly grew after 10 min, could be identified as a gas phase or weakly adsorbed NO_2 [19,46]. Similarly, for WI–$Ce_{0.25}TiO_2$ catalyst (see Fig. 8b), the bands at 1601 cm^{-1} and 1554 cm^{-1} were due to bridged and bidentate nitrates, respectively, whist the bands at 1375 and 1365 cm^{-1} could be assigned to *cis*-$N_2O_2^-$. The band at 1246 cm^{-1} was attributed to nitrite species whilst the new bands at 1298 cm^{-1} could be attributed to monodentate nitrate species based on the literatures [47,48]. By comparing the DRIFT spectra of the two catalysts, it could be concluded that the CeO_2 did provide great numbers of NO adsorption sites over the catalysts, generating significant nitrite species as well as NO_2. However, it can be seen that the formation of NO_2 and nitrite species was more evident on SC–$Ce_{0.25}TiO_2$ catalyst than that on WI–$Ce_{0.25}TiO_2$ catalyst. This could be attributed to the presence of abundant surface oxygen vacancies on the SC–$Ce_{0.25}TiO_2$ catalyst but needed further characterizations.

Qi and Yang [46] have argued that the NO_2 and nitrite species could be effectively involved in the SCR reaction while the nitrate species were hardly reacted with ammonia. To further confirm this, DRIFT study on the reaction between ammonia and nitrogen oxides ad-species over the two catalysts was then performed. The catalysts were purged with $NO_2 + O_2$ for 30 min followed by NH_3 being introduced. As shown in Fig. 9, the SC–$Ce_{0.25}TiO_2$ catalyst showed the band attributed to NO_2 (1618 cm^{-1}) and nitrite species (1234 cm^{-1}), both of which were decreased after NH_3 was passed over (see Fig. 9a), implying a reaction was occurred between the NH_3 and NO_2/nitrite species. The nitrate species did not showed great changes, indicating the non-involvement of the nitrate species in the SCR reaction. Similar results were also observed for WI–$Ce_{0.25}TiO_2$ catalyst (see Fig. 9b). In addition, the new bands emerged at 1691/1734 cm^{-1} and 1207/1186 cm^{-1} were all due to the NH_3 ad-species [49–51]. This result confirmed the involvements of NO_2 and nitrite species in the SCR reaction, where the NO was readily adsorbed on the surface oxygen vacancy sites of the Ce_xTiO_2 catalysts and then oxidized into NO_2 and/or transferred to nitrite species, reacting with the absorbed NH_3 to form N_2 and H_2O. The presence of enriched surface oxygen vacancies (as resulted by the SMSI) could facilitate the formation of NO_2 and nitrite species, leading to remarkable SCR performances for SC–Ce_xTiO_2 catalysts (see Fig. 2).

In addition, we have conducted a preliminary test at 300 °C to evaluate the effect of SO_2 on the performance of the developed SC–$Ce_{0.25}TiO_2$ catalyst where 100 ppm SO_2 was introduced in addition to the 5 vol% H_2O. As shown in Supplementary Fig. S5, the SC–$Ce_{0.25}TiO_2$ catalyst revealed a gradually decreased NO conversion. After switching off H_2O input, the NO conversion was maintained and recovered step by step after further stopping SO_2 inlet. This result clearly indicated that the deposit of ammonium sulphate was the main cause for the loss of SCR activity. Although under H_2O and SO_2 coexistence condition, the developed SC–$Ce_{0.25}TiO_2$ catalyst had shown a relatively similar performance to Ce–W–TiO_2 catalyst that was previously developed [37], further modifications are still urgently needed with an aim to enhance the poisoning resistance of the catalysts.

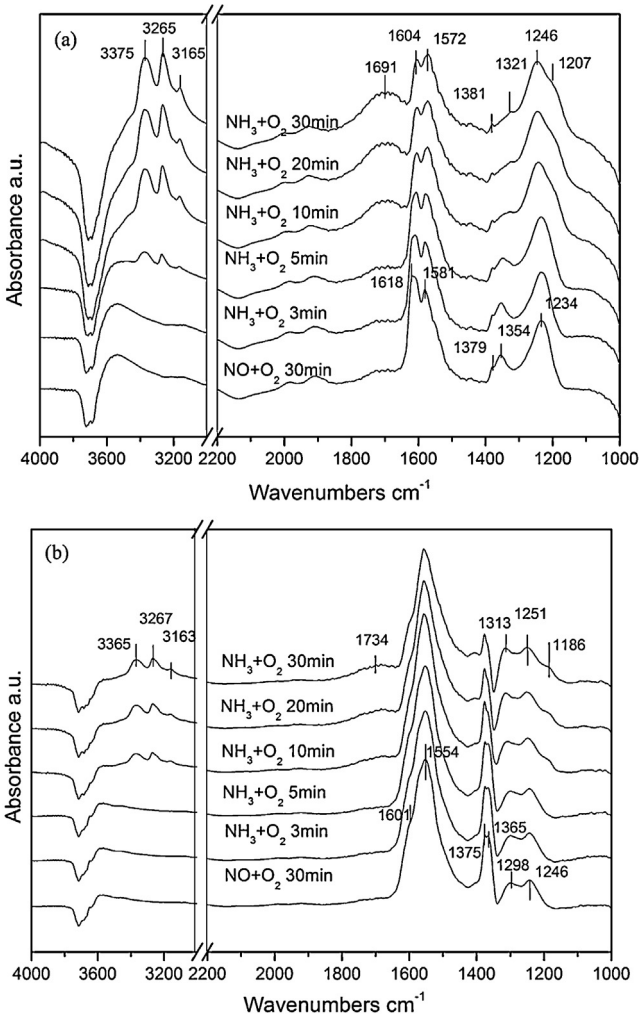

Fig. 9. DRIFT spectra taken at 250 °C upon passing 1000 ppm NH_3 + 3% O_2/He over the NO + O_2 pre-sorbed on (a) SC–$Ce_{0.25}TiO_2$ and (b) WI–$Ce_{0.25}TiO_2$ at different time.

4. Conclusions

In this paper, we demonstrated the feasibility of the CHFS route in the syntheses of SMSI catalysts for SCR application. The resulted SMSI in the SC–Ce_xTiO_2 catalysts had yielded enriched oxygen vacancies on catalyst surface, which facilitated the formation of NO_2 and nitrite species, hence enhancing their SCR performances. The SMSI had also lowered the NH_3 oxidation ability of the CeO_2, effectively extending the SCR operation temperature window for the catalysts. However, further modifications aiming to enhance the poisoning resistance (under H_2O and SO_2 coexistent condition) of the catalyst are still urgently required, where several approaches are currently under investigation, the results of which will be reported in due course. We expect that this work could shed some lights on the development of feasible preparative routes for the syntheses of advanced SMSI catalysts for SCR application.

Author contributions

The manuscript was written through contributions of all authors. All authors have given approval to the final version of the manuscript.

Acknowledgements

The work is financially supported by Key Project of Zhejiang Provincial Science and Technology Program (Grant no. 2012C03003-4), Zhejiang Provincial Natural Science Foundation of China (Grant no. LQ12E08011), Zhejiang Provincial "151" Talents Program and Changjiang Scholar Incentive Program (2009), Ministry of Education, P. R. China.

Appendix A. Supplementary data

Supplementary data associated with this article can be found, in the online version, at http://dx.doi.org/10.1016/j.apcatb.2014.06.022.

References

[1] L.J. Alemany, F. Berti, G. Busca, G. Ramis, D. Robba, G.P. Toledo, M. Trombetta, Appl. Catal., B: Environ. 10 (1996) 299–311.
[2] L. Casagrande, L. Lietti, I. Nova, P. Forzatti, A. Baiker, Appl. Catal., B: Environ. 22 (1999) 63–77.
[3] Z. Liu, S. Zhang, J. Li, L. Ma, Appl. Catal., B: Environ. 144 (2014) 90–95.
[4] B. Thirupathi, P.G. Smirniotis, J. Catal. 288 (2012) 74–83.
[5] M. Casapu, O. Kröcher, M. Elsener, Appl. Catal., B: Environ. 88 (2009) 413–419.
[6] D. Zhang, L. Zhang, C. Fang, R. Gao, Y. Qian, L. Shi, J. Zhang, RSC Adv. 3 (2013) 8811–8819.
[7] W. Shan, F. Liu, H. He, X. Shi, C. Zhang, ChemCatChem 3 (2011) 1286–1289.
[8] T. Adschiri, K. Kanazawa, K. Arai, J. Am. Ceram. Soc. 75 (1992) 2615–2618.
[9] Y. Hakuta, T. Adschiri, H. Hirakoso, K. Arai, Fluid Phase Equilib. 158–160 (1999) 733–742.
[10] Y. Hakuta, K. Seino, H. Ura, T. Adschiri, H. Takizawa, K. Arai, J. Mater. Chem. 9 (1999) 2671–2674.
[11] J.A. Darr, M. Poliakoff, Chem. Rev. 99 (1999) 495–542.
[12] A. Cabanas, J.A. Darr, M. Poliakoff, E. Lester, Chem. Commun. (2000) 901–902.
[13] F. Cansell, C. Aymonier, A. Loppinet-Serani, Curr. Opin. Solid State Mater. Sci. 7 (2003) 331–340.
[14] X.-R. Ye, Y. Lin, C. Wang, M.H. Engelhard, Y. Wang, C.M. Wai, J. Mater. Chem. 14 (2004) 908.
[15] A. Cabanas, J.A. Darr, E. Lester, M. Poliakoff, Chem. Commun. (2000) 901–902.
[16] X. Weng, B. Perston, X.Z. Wang, I. Abrahams, T. Lin, S. Yang, J.R.G. Evans, D.J. Morgan, A.F. Carley, M. Bowker, J.C. Knowles, I. Rehman, J.A. Darr, Appl. Catal., B: Environ. 90 (2009) 405–415.
[17] X. Weng, J. Zhang, Z. Wu, Y. Liu, H. Wang, J.A. Darr, Appl. Catal., B: Environ. 103 (2011) 453–461.
[18] X. Weng, J. Zhang, Z. Wu, Y. Liu, H. Wang, J.A. Darr, Green Chem. 13 (2011) 850.
[19] P. Li, Y. Xin, Q. Li, Z. Wang, Z. Zhang, L. Zheng, Environ. Sci. Technol. 46 (2012) 9600–9605.
[20] Z. Liu, Y. Yi, J. Li, S.I. Woo, B. Wang, X. Cao, Z. Li, Chem. Commun. 49 (2013) 7726–7728.
[21] W. Shan, F. Liu, H. He, X. Shi, C. Zhang, Catal. Today 184 (2012) 160–165.
[22] W. Xu, H. He, Y. Yu, J. Phys. Chem. C 113 (2009) 4426–4432.
[23] W. Xu, Y. Yu, C. Zhang, H. He, Catal. Commun. 9 (2008) 1453–1457.
[24] X. Gao, Y. Jiang, Y. Fu, Y. Zhong, Z. Luo, K. Cen, Catal. Commun. 11 (2010) 465–469.
[25] X. Gao, Y. Jiang, Y. Zhong, Z. Luo, K. Cen, J. Hazard. Mater. 174 (2010) 734–739.
[26] X. Weng, J. Zhang, Z. Wu, Y. Liu, Catal. Today 175 (2011) 386–392.
[27] Q. Yuan, H.-H. Duan, L.-L. Li, Z.-X. Li, W.-T. Duan, L.-S. Zhang, W.-G. Song, C.-H. Yan, Adv. Mater. 22 (2010) 1475–1478.
[28] W.F. Zhang, Y.L. He, M.S. Zhang, Z. Yin, Q. Chen, J. Phys. D: Appl. Phys. 33 (2000) 912.
[29] G. Vlaic, R. Di Monte, P. Fornasiero, E. Fonda, J. Kašpar, M. Graziani, J. Catal. 182 (1999) 378–389.
[30] B. Choudhury, B. Borah, A. Choudhury, Mater. Sci. Eng., B 178 (2013) 239–247.
[31] B. Choudhury, A. Choudhury, Mater. Chem. Phys. 132 (2012) 1112–1118.
[32] S. Yang, W. Zhu, Z. Jiang, Z. Chen, J. Wang, Appl. Surf. Sci. 252 (2006) 8499–8505.
[33] X. Liu, K. Zhou, L. Wang, B. Wang, Y. Li, J. Am. Chem. Soc. 131 (2009) 3140–3141.
[34] M. Kang, E.D. Park, J.M. Kim, J.E. Yie, Appl. Catal., A: Gen. 327 (2007) 261–269.
[35] Z. Wu, R. Jin, H. Wang, Y. Liu, Catal. Commun. 10 (2009) 935–939.
[36] F. Fally, V. Perrichon, H. Vidal, J. Kaspar, G. Blanco, J.M. Pintado, S. Bernal, G. Colon, M. Daturi, J.C. Lavalley, Catal. Today 59 (2000) 373–386.
[37] W. Shan, F. Liu, H. He, X. Shi, C. Zhang, Appl. Catal., B: Environ. 115–116 (2012) 100–106.
[38] F. Liu, H. He, C. Zhang, W. Shan, X. Shi, Catal. Today 175 (2011) 18–25.
[39] V. Sanchez-Escribano, T. Montanari, G. Busca, Appl. Catal., B: Environ. 58 (2005) 19–23.
[40] X. Wang, A. Shi, Y. Duan, J. Wang, M. Shen, Catal. Sci. Technol. 2 (2012) 1386.
[41] C.-C. Chao, J.H. Lunsford, J. Am. Chem. Soc. 93 (1971) 71–77.
[42] N. Tang, Y. Liu, H. Wang, Z. Wu, J. Phys. Chem. C 115 (2011) 8214–8220.
[43] B. Azambre, L. Zenboury, A. Koch, J.V. Weber, J. Phys. Chem. C 113 (2009) 13287–13299.
[44] S. Xie, J. Wang, H. He, J. Mol. Catal. A: Chem. 266 (2007) 166–172.
[45] M. Machida, M. Uto, D. Kurogi, T. Kijima, J. Mater. Chem. 11 (2001) 900–904.
[46] G. Qi, R.T. Yang, R. Chang, Appl. Catal., B: Environ. 51 (2004) 93–106.
[47] Z. Wu, B. Jiang, Y. Liu, H. Wang, R. Jin, Environ. Sci. Technol. 41 (2007) 5812–5817.
[48] M. Kantcheva, J. Catal. 204 (2001) 479–494.
[49] G. Ramis, M. Angeles Larrubia, J. Mol. Catal. A: Chem. 215 (2004) 161–167.
[50] W. Shan, F. Liu, H. He, X. Shi, C. Zhang, Chem. Commun. 47 (2011) 8046.
[51] L. Chen, J. Li, M. Ge, Environ. Sci. Technol. 44 (2010) 9590–9596.